IDEAL MHD STABILITY PROPERTIES OF PRESSURE DRIVEN MODES IN LOW SHEAR TOKAMAKS

J. MANICKAM, N. POMPHREY
Princeton Plasma Physics Laboratory,
Princeton, New Jersey

A.M.M. TODD
Grumman Corporation,
Plainsboro, New Jersey

United States of America

ABSTRACT. The role of shear in determining the ideal MHD stability properties of tokamaks is discussed. In particular, the effects of low shear within the plasma upon pressure driven modes are assessed. The standard ballooning theory is shown to break down as the shear is reduced, and the growth rate is shown to be an oscillatory function of n, the toroidal mode number, treated as a continuous parameter. The oscillations are shown to depend on both the pressure profile and the safety factor profile. When the shear is sufficiently weak, the oscillations can result in bands of unstable n-values, which are present even when the standard ballooning theory predicts complete stability. These instabilities are named 'infernal modes'. The occurrence of these instabilities at integer n is shown to be a sensitive function of the q-axis, raising the possibility of a sharp onset as the plasma parameters evolve.

1. INTRODUCTION

The importance of shear in determining the ideal MHD stability properties of tokamaks is well recognized. The general understanding of its role was largely based on simple cylindrical models, for instance presented in the review articles of Wesson [1] and Friedberg [2]. More recently it has become clear that careful numerical treatment is essential to define the effects of shear on the stability of ideal MHD modes [3–8]. This understanding has been used to propose paths to second regions of stability [9, 10]. However, there remain areas of imperfect understanding, one of which we intend to explore in this report. In particular, we assess the role of low shear on the stability of pressure driven modes. The shear generally refers to a gradient in the safety factor profile. In some situations it is represented by the ratio of q-edge to q-axis; it can also be defined as $\psi\, dq/d\psi$ ($\equiv \psi q'$), which will be referred to here as the global shear. Another form that plays an important role in high-n ballooning modes is the local shear, a quantity which measures the skewness of the magnetic field lines on nearby surfaces and which has been identified as playing a critical role in determining stability to ballooning modes [7].

In this report we are largely concerned with the global shear and its effect on internal pressure driven instabilities. These modes have been analysed extensively using analytical and numerical methods. In general, when the toroidal mode number, n, is large, the ballooning theory [11–13] is applicable. In this approach it is observed that ballooning modes can be constructed from the overlap of many localized Fourier modes peaking on their own rational surfaces. In the high-n limit, this also implies a radial localization of the mode, which permits the reduction of the equations to an ordinary differential equation valid on each flux surface. Thus, each flux surface can be independently tested for stability to high-n ballooning modes. In contrast, when n is small (~ 1), the numerical approach of solving the full two-dimensional ideal MHD equations [14, 15] is required. This approach can, in principle, be extended to high n. However, in practice, mode resolution and hence computer memory requirements restrict the analysis to $n \lesssim 10$. Ballooning theory has been modified to include finite-n corrections, and has been shown to agree with the detailed MHD approach down to $n \sim 5$ [16–18]. Ballooning theory predicts that the largest n modes are the most unstable, and that as n is decreased the growth rate decreases monotonically. In certain circumstances this picture is modified to include an oscillatory dependence of growth rate on mode number. This is shown explicitly in Ref. [16], where n is treated as a continuous variable. The oscillatory behaviour has been independently described

by Hastie and Taylor [19], who attribute the oscillations to a breakdown of the standard ballooning theory when the global shear becomes weak. They also propose a new theory which would supersede the standard ballooning theory in these conditions. They postulate regions of validity of their theory and show that in the high-n limit the standard ballooning theory is recovered. This paper treats the same problem. In particular, we verify the Hastie–Taylor theory when the shear is weak, and we also show that if the shear is further reduced, even this theory breaks down; instabilities are observed, which can be present even when the standard ballooning theory predicts complete stability. We call these instabilities 'infernal modes'. We discuss them and analyse the role of both p′ ($\equiv dp/d\psi$) and q′ in driving the instability.

Weak shear near the axis is often accompanied by strong shear near the plasma edge, which has a strong stabilizing influence on the external kink mode. In this situation the threshold for instability can be at very large values of beta ($\equiv 2\langle p\rangle/\langle B^2\rangle$) and the instability can take the form of an internal mode, where the boundary conditions play a minor role in determining stability. In particular, when q′ is small and p′ is large near the axis, the resulting instability may be dominated by a low-m (~ 1) Fourier component, even when there is no q = 1 surface inside the plasma. This is significant, in that it represents a fairly typical operating scenario for tokamaks, suggesting that these instabilities may play an important role in present high beta tokamaks.

In the following sections we first describe the equilibrium models and numerical methods used in this study. Then we present our results, highlighting several of the issues raised here. Finally, we present our observations and conclusions.

2. EQUILIBRIUM MODEL AND NUMERICAL METHODS

This study focuses on the influence of shear on stability to pressure driven modes. Since these are essentially profile related effects, we choose a simple geometry for the plasma and consider a circular cross-sectional tokamak with an aspect ratio R/a = 4. The q-profile is specified to have the functional form

$$q = q_0 + q_1 \psi^{\alpha_q}$$

so that q_0 determines the q-axis, and q-edge is $q_0 + q_1$. We have chosen $q_0 = 1.05$, and $q_1 = 2.05$ for the majority of cases studied here; exceptions will be noted. The flux label ψ is normalized to have a value of zero at the magnetic axis and to be unity at the plasma edge; α_q is used to vary the shear. When α_q is greater than unity, which is the case for this study, the shear has its minimum near the axis. If q-axis and q-edge are held fixed as α_q is increased, the effect is to weaken simultaneously the shear near the axis and to increase the shear near the edge. Figure 1 shows the q-profile for several values of α_q. The main body of results requires a large pressure gradient in regions of low shear, hence we adopt a pressure profile of the form

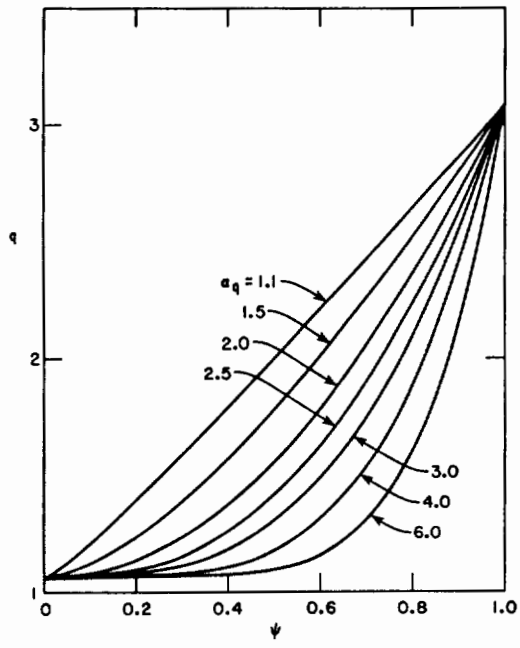

FIG. 1. Safety factor profiles $q(\psi)$ used in this study. $q_{axis} = 1.05$, $q_{edge} = 3.10$ and α_q varies between 1.1 and 6.0.

$$p = p_0 (1-\psi^{\alpha_2})^{\alpha_1}$$

with $\alpha_1 = 4$ and $\alpha_2 = 1.5$. The central pressure, p_0, is adjusted to yield the desired value of β. The profile and its derivative are shown in Fig. 2(a). We choose β so that, as α_q is varied, the resulting equilibria remain unstable to ballooning modes. A convenient choice for our study is to set β equal to 1.5%. The equilibrium calculations are made with a flux co-ordinate solver [20] on a mesh with 50 radial and 100 poloidal intervals. This is then interpolated onto a finer grid with

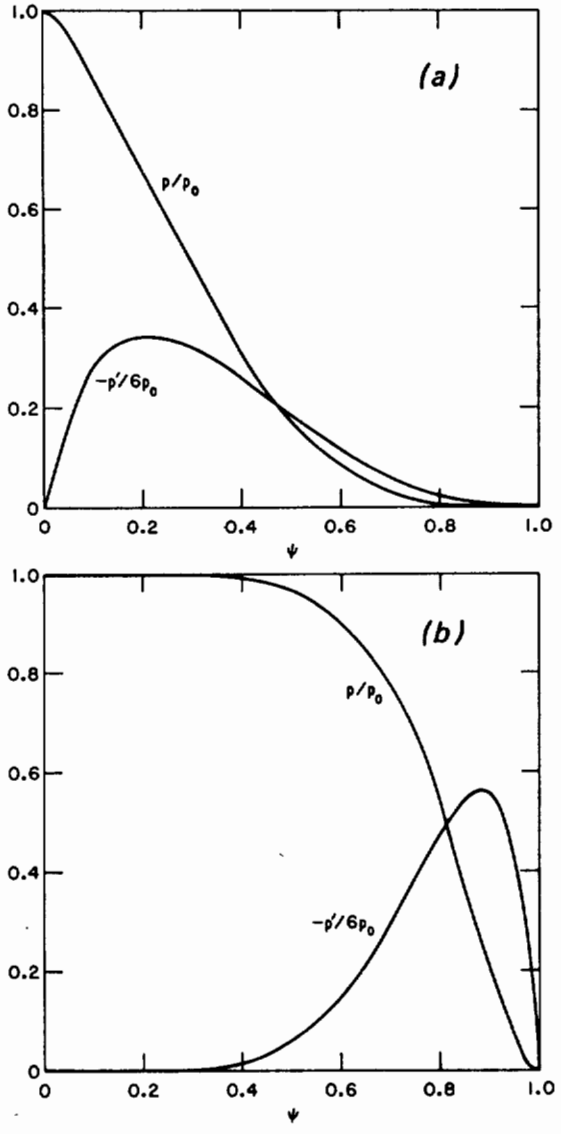

FIG. 2. Pressure profile and its derivative corresponding to: (a) $\alpha_1 = 4.0$, $\alpha_2 = 1.5$, used for most of the studies reported. (b) $\alpha_1 = 2.0$, $\alpha_2 = 6.0$, with the derivative shifted to the outside.

200 radial and 128 poloidal intervals for the stability analysis, which is conducted using the PEST code [14]. This mesh is also used for the standard WKB ballooning code [16]. In this study we consider toroidal mode numbers up to 12, which requires an ability to resolve poloidal harmonics with a value up to 40. To ensure this resolution, at the higher values of n, we double the number of poloidal mesh points (256). An examination of the resulting eigenvectors shows the adequacy of these meshes. Finally, we note that, since we intend to compare eigenvalues of different toroidal modes, we cannot use the scalar version of PEST [21]; instead, we use the proper kinetic energy normalization of the complete representation [14].

Our procedure is to generate several equilibria for different values of α_q, keeping β equal to 1.5%, and then analyse them for stability to ballooning modes. A conducting shell is placed at the plasma edge and the radial perturbation is required to vanish there. We utilize the WKB code to determine the stability properties according to the standard ballooning theory, including predictions of the critical n for instability using the quantization condition where applicable. We then analyse the same equilibria using the PEST code, treating the toroidal mode number n as a continuous real variable, rather than as an integer. This is justified by the fact that n appears as a fixed expansion parameter in the ballooning theory. Further, it generally appears in stability analysis as a product of n and q, and we can interpret non-integer n for a certain value of q, as an integer n for a slightly modified q-profile. We plot the growth rate as a function of n and compare the results with the predictions of the different ballooning theories.

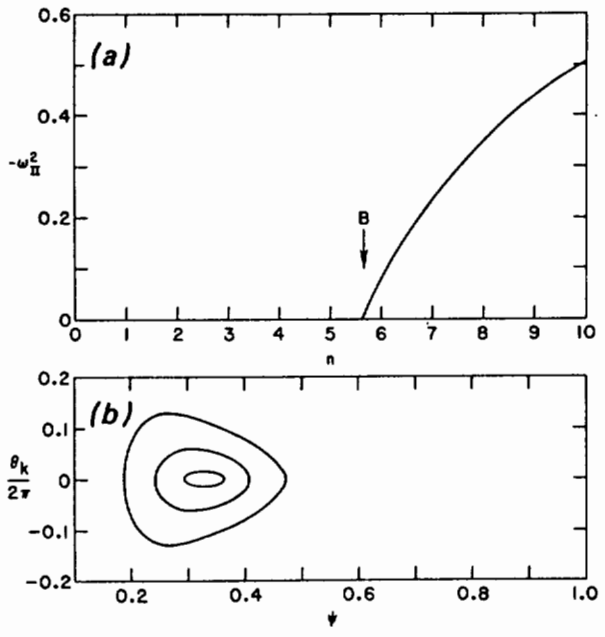

FIG. 3. (a) Variation of the growth rate (ω^2), in arbitrary units, with the toroidal mode number (n) for the q-profile with $\alpha_q = 1.5$, $\beta = 0.8\%$. B marks the critical-n for marginal stability as determined by a WKB code.
(b) Contours of constant growth rate, $\lambda(\psi,\theta_k)$, from the WKB code. The outermost contour signifies marginal stability, $\lambda = 0$.

3. RESULTS

The PEST code, being an exact code with no approximations or orderings, will be used to represent the true situation. We will then compare the results of the ballooning mode analysis with the PEST results. We commence with a case that conforms to standard ballooning theory. For this we choose α_q equal to 1.5, $\beta \sim 0.8\%$, and the pressure profile of Fig. 2(a). Figure 3(a) shows the results from the PEST-II code [21], plotting the growth rate as a function of n. (The PEST-II code has been used here since we only look for the point of marginal stability; in all subsequent studies we use the PEST-I code [14].) An extrapolation to zero growth rate shows a critical n of 5.6. The results of ballooning mode analysis are shown in Fig. 3(b), where we plot contours of constant growth rate λ in the ψ–θ_k plane; θ_k represents the angle between the radial component of the wave vector, k_q, and the component parallel to the field line, k_α. Details of this can be found in Ref. [16]. In the present paper we plot $\lambda(\psi,\theta_k)$ rather than $\lambda(q,\theta_k)$ to enhance the visibility of the unstable regions. Using a WKB quantization condition, it is then possible to determine the value of the critical n above which the mode is unstable. In this example the critical n has the value 5.7, which is in virtual coincidence with the value predicted by the PEST analysis. This confirms the general validity of the codes and procedures used in this study, and reaffirms the possibility of correctly analysing moderate-n ballooning modes in a standard

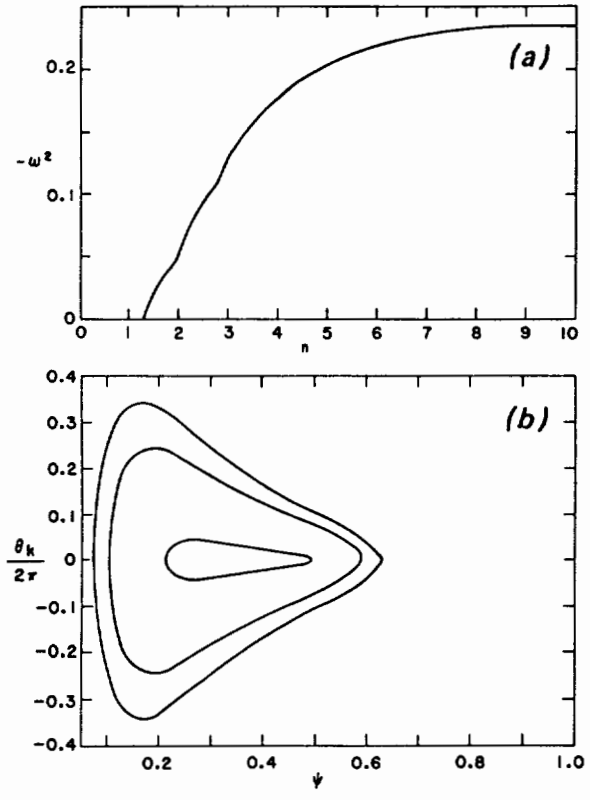

FIG. 4. (a) ω^2 versus n for α_q = 1.1, β = 1.5%. (b) Contours of $\lambda(\psi,\theta_k)$.
(ω^2 is normalized in units of the poloidal Alfvén frequency for this and subsequent figures.)

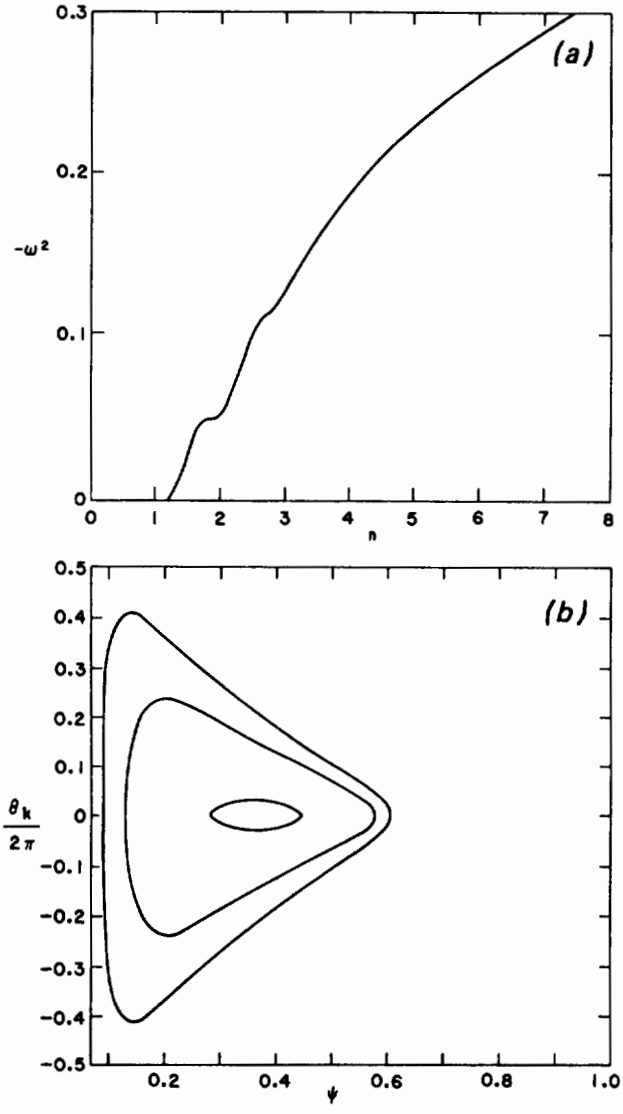

FIG. 5. (a) ω^2 versus n for α_q = 1.5, β = 1.5%. (b) Contours of $\lambda(\psi,\theta_k)$.

situation with both the ballooning code and the PEST code. We now proceed to the analysis of weak shear equilibria.

The role of the shear is central to these results; hence we fix the pressure profile and adjust p_0 such that β remains approximately constant at a value of 1.5%. We then vary the shear profile parameter α_q over a wide range to modify the shear. The results are shown in a form similar to that of Fig. 3. In each case we show the variation of the growth rate in units of the poloidal Alfvén frequency, as obtained from the PEST code, with the toroidal mode number n. Corresponding to the PEST analysis we also show the ballooning code analysis as contours in the ψ–θ_k plane. It will be noted that some of the contours appear as open lines when a separatrix is present. In this situation the usual method of determining the critical n from the area of the closed contour corresponding to $\lambda = 0$ breaks down, and the critical n reported must be considered as approximate. The results for α_q equal to 1.1, 1.5, 2.0, 2.5, 3.0, 4.0 and 6.0 are shown in Figs 4–10. The PEST results for this sequence of equilibria show a distinct progression, from a relatively smooth monotonic dependence of the growth rate on n, to a strongly oscillatory function, which eventually leads to alternating stable and unstable bands in n. We attribute this to the gradual reduction of the shear, q′, in the vicinity of the driving force — the pressure gradient. We note that when α_q is less than 3, for n-values higher than 5 there is a monotonic variation of the growth rate, and for lower n-values there are oscillations. This result is in agreement with the low-

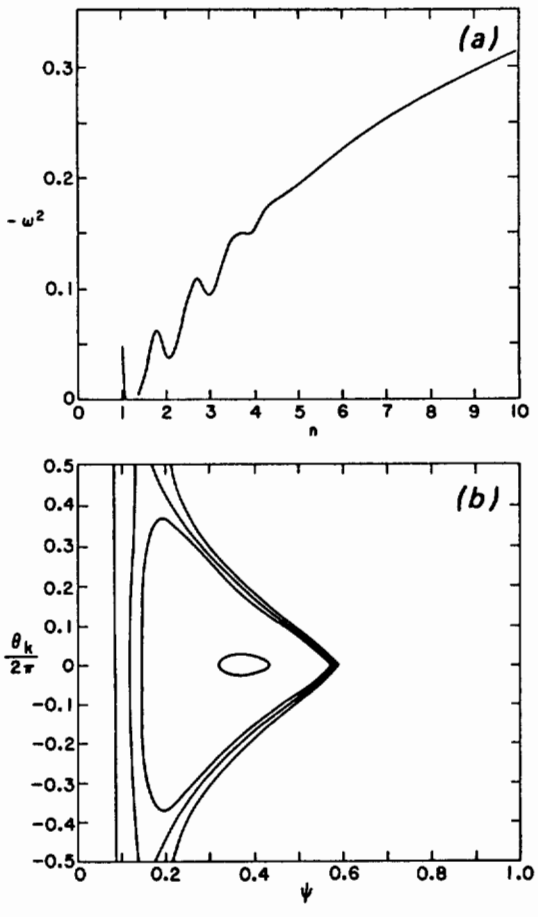

FIG. 6. (a) ω^2 versus n for $\alpha_q = 2.0$, $\beta = 1.5\%$. (b) Contours of $\lambda(\psi,\theta_k)$.

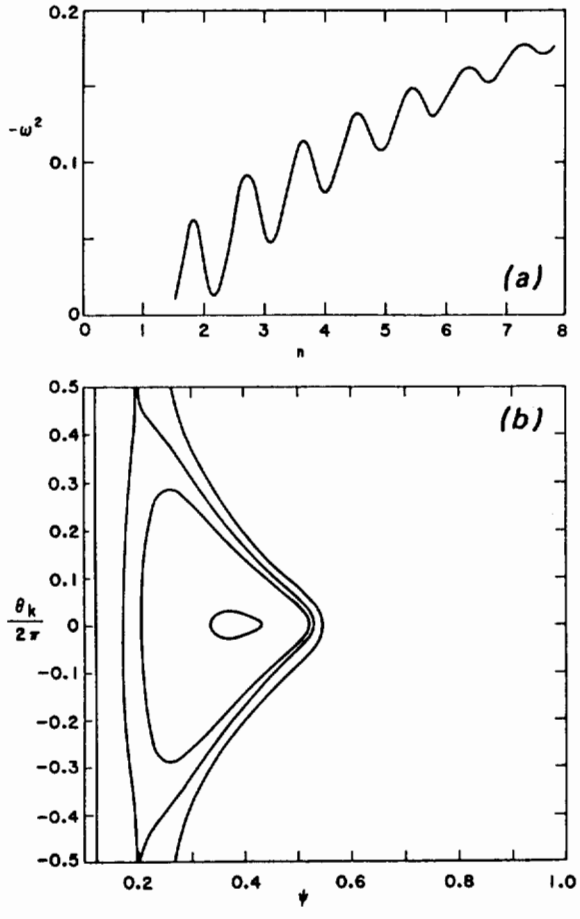

FIG. 7. (a) ω^2 versus n for $\alpha_q = 2.5$, $\beta = 1.5\%$. (b) Contours of $\lambda(\psi,\theta_k)$.

shear theory of Ref. [19], which predicts that when q′ is small, a critical value of n exists above which standard ballooning theory would apply; below this value, oscillations in the growth rate would be expected. This general picture is clearly supported here and will be discussed in greater detail below. As α_q increases, the oscillations are extended to larger values of n; the PEST code is limited to n-values of about 10 and hence the expected monotonic variation at high n is not observed in these cases.

The ballooning analysis of these equilibria shows a distinct topological change in the constant λ contours as α_q is increased. We note that the region of instability extends to θ_k equal to π, and a separatrix appears. In Ref. [16] it is argued that the appearance of this separatrix is responsible for the oscillations in the growth rate, which would peak whenever a rational surface coincided with q_x, the surface corresponding to the separatrix. Figure 5 shows that mild oscillations can be present even when there is no separatrix. We believe this is due to the high beta value which, for this α_q, is considerably higher than the threshold value for marginal stability. This characteristic appearance of a separatrix is an extremely useful diagnostic for detecting the presence of oscillations. Finally, in relation to this set of figures we comment that when the oscillations are limited in size and range there is some agreement between the critical n as determined by the PEST code and the WKB ballooning code. When α_q is 3 or greater and the oscillations are strong, there is no correlation whatsoever between the two codes. In fact, the concept of the critical n is itself questionable.

We have explored the role of the shear in determining the conditions for oscillations. We now analyse the role of the pressure profile. The profile used in the first set of equilibria has its largest gradient at ψ of approximately 0.2, as shown in Fig. 2(a). This is also the region where the shear is reduced the most as α_q is changed. We now choose the pressure profile so that it peaks further out, nearer to the plasma edge, by setting $\alpha_1 = 2.0$ and $\alpha_2 = 6.0$. This puts the maximum of p′ at $\psi = 0.9$, as shown in Fig. 2(b). The q-profile is chosen to be the same as the one analysed in Fig. 9, with $\alpha_q = 4$. Figure 11 shows the stability analysis of

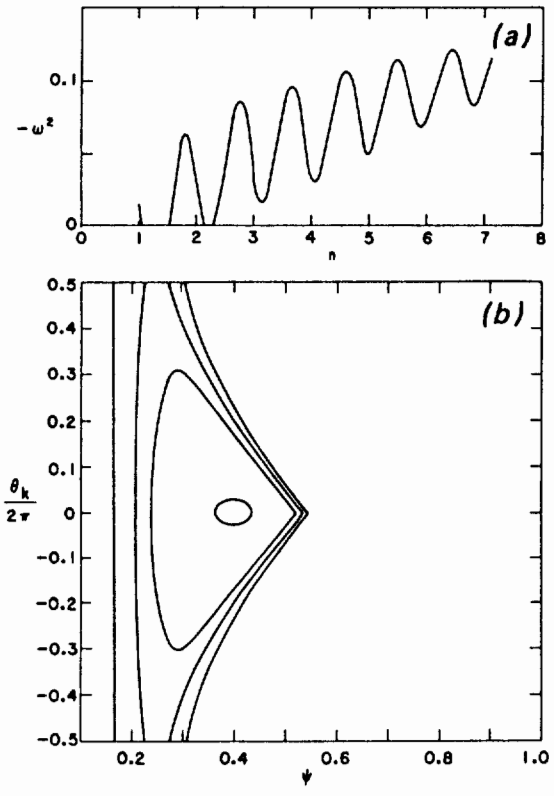

FIG. 8. (a) ω^2 versus n for $\alpha_q = 3.0$, $\beta = 1.5\%$. (b) Contours of $\lambda(\psi,\theta_k)$.

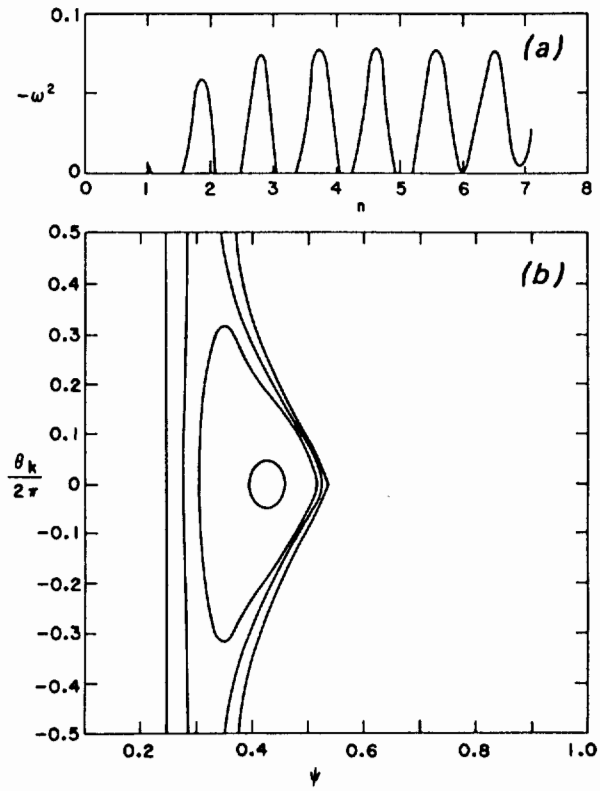

FIG. 9. (a) ω^2 versus n for $\alpha_q = 4.0$, $\beta = 1.5\%$. (b) Contours of $\lambda(\psi,\theta_k)$.

this equilibrium, Fig. 11(a) giving the PEST results and Fig. 11(b) the ballooning results. These are to be compared with Fig. 9. The oscillations have disappeared completely and we recover a smooth monotonic dependence of the growth rate on n. This suggests that for oscillations to appear it is necessary to have both low shear and a large enough p′ in the regions of low shear. In fact, on the basis of the results of Figs 3 and 5, which are for the same q and pressure profile shapes and which differ only in the beta (0.8% and 1.5%, respectively), we note that even if q′ is moderate, the oscillations can be made to appear if beta is increased. However, once instability is reached, it is irrelevant to increase beta any further, and the issue of oscillations at higher beta is of academic interest. On the other hand, if oscillations are present close to the threshold of instability, they may have practical consequences. This will become apparent when we study an equilibrium that is stable to infinite-n ballooning modes. We do this by choosing an equilibrium with parameters similar to those of Fig. 10 (pressure profile of Fig. 2(a) and $\alpha_q = 6$), and reducing beta until we obtain stability to ballooning modes; this occurs at $\beta = 1\%$. This equilibrium is then analysed to obtain the results shown in Fig. 12. Since this is stable to ballooning modes with $n = \infty$, there is no ψ–θ_k contour plot. We note the existence of unstable bands at low n, which vanish when n gets sufficiently large. This represents a case where the ballooning mode results would be misleading, as they would infer stability when in fact there are several low-n internal pressure driven 'ballooning like' modes. The modes that persist even after the high-n modes are stabilized are termed 'infernal modes'.

For the results presented here, a simple parametrization of the q-profile has been used. This form has the disadvantage that the shear throughout the plasma is controlled by a single parameter. Thus, if the shear near the axis is reduced, this increases the shear near the edge. We now introduce a parametrization of q of the form

$$q = q_0 + q_1 \psi^{\alpha_q} \qquad \text{for } 0 < \psi < \psi_m$$

$$q = q_0 + q_1 \psi^{\alpha_q} + q_2(\psi-\psi_m)^{\alpha_{q2}} \qquad \text{for } \psi_m < \psi < 1$$

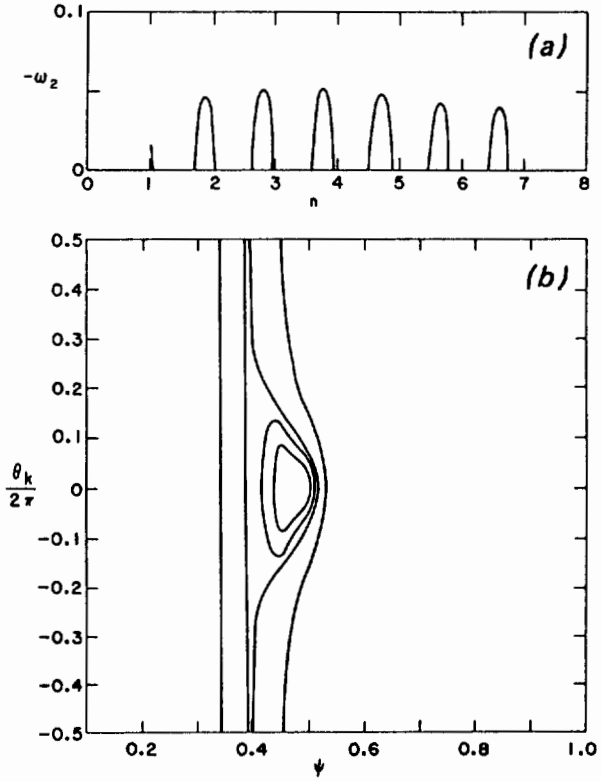

FIG. 10. (a) ω^2 versus n for $\alpha_q = 6.0$, $\beta = 1.5\%$.
(b) Contours of $\lambda(\psi,\theta_k)$.

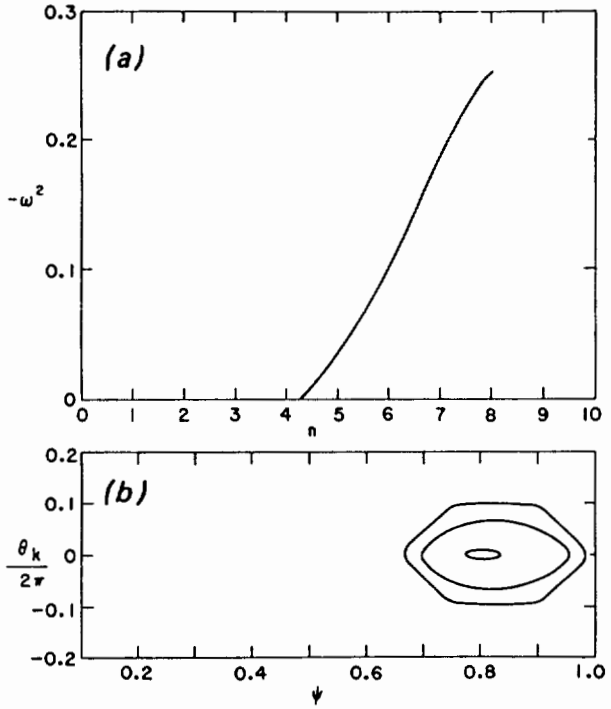

FIG. 11. (a) ω^2 versus n for $\alpha_q = 4.0$, $\beta = 1.5\%$.
The pressure profile of Fig. 2(b) is chosen to minimize the gradient in the region of low shear.
(b) Contours of $\lambda(\psi,\theta_k)$.

This form permits us to lower the shear in the region $0 < \psi < \psi_m$, without a large shear outside it being required, and it more closely represents experimental profiles. Figure 13 shows the q, p and J_ϕ profiles as a function of the distance from the major axis for this profile when q_0, q_1, q_2, α_q, α_{q2} and ψ_m have the values 1.05, 0.15, q_2, 1.1, 2.8 and 0.3, respectively. Note that the value of q_2 is adjusted so that the q-edge is 3.1. The pressure profile parameters are the same as those used earlier, i.e. $\alpha_1 = 4$ and $\alpha_2 = 1.5$. With p_0 adjusted to give $\beta = 1.45\%$, we find the ω^2 dependence shown in Fig. 14(a) and the ballooning stability shown in Fig. 14(b). As before, we note the presence

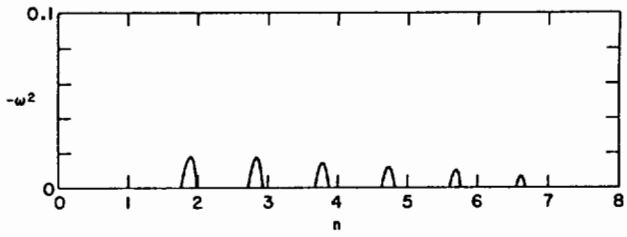

FIG. 12. ω^2 versus n for $\alpha_q = 6.0$, $\beta = 1.0\%$; pressure profile of Fig. 2(a). This equilibrium is stable to high-n ballooning modes. The low-n modes are termed 'infernal modes'.

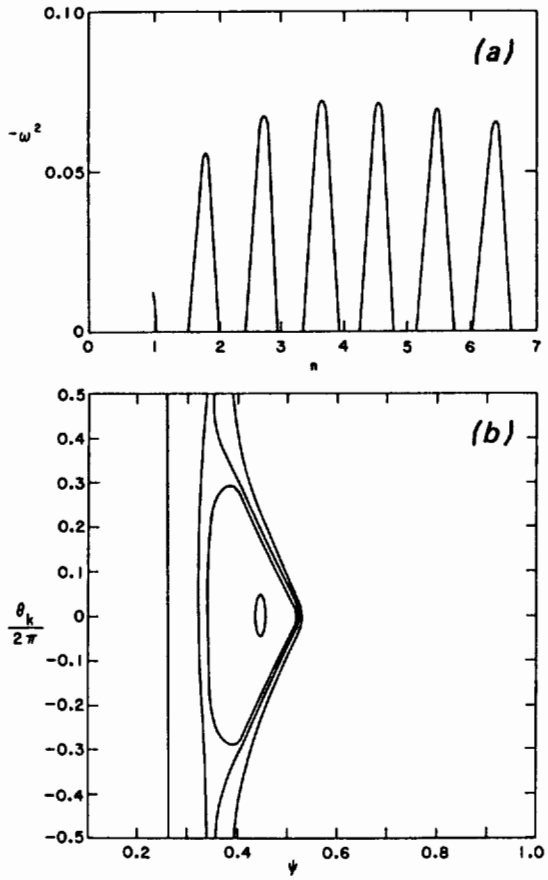

FIG. 14. (a) ω^2 versus n for the equilibrium of Fig. 13, when $\beta = 1.45\%$.
(b) Contours of $\lambda(\psi,\theta_k)$.

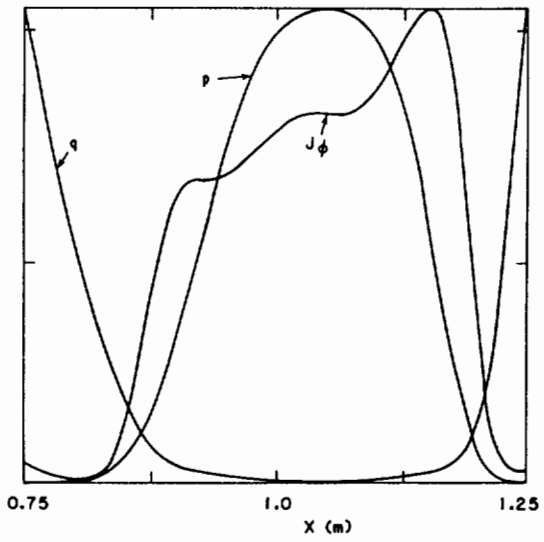

FIG. 13. Current density, pressure profiles and q-profiles for a model equilibrium that mimics typical experimental profiles. The units are arbitrary, $q_{axis} = 1.05$, $q_{edge} = 3.1$ and $\beta = 1.45\%$.

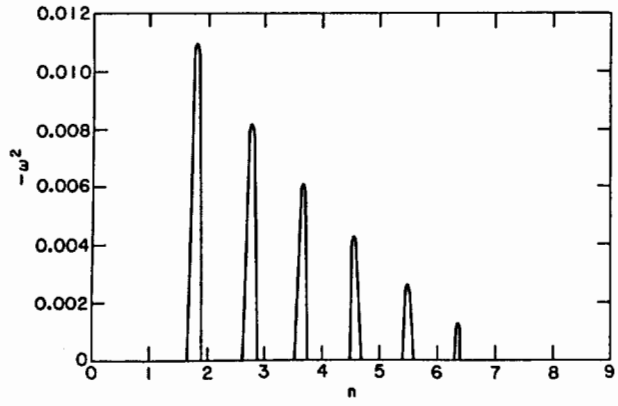

FIG. 15. ω^2 versus n for the equilibrium parameters of Fig. 13, with $\beta = 0.8\%$, showing the 'infernal modes' where high n is stable.

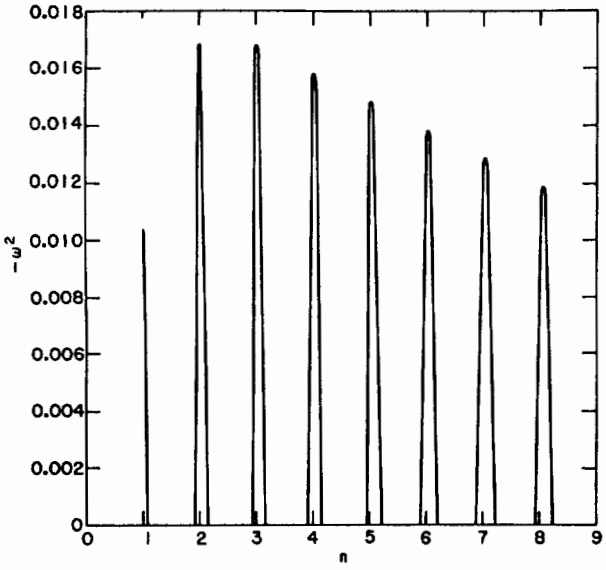

FIG. 16. ω^2 versus n for the equilibrium of Fig. 15, with the toroidal field scaled so that q_{axis} is 0.96 instead of 1.05. Note the resonances of the instabilities with integer n.

of the separatrix and the sharp resonances in the growth rate for particular values of n. The peaks do not coincide with integer n and, in fact, only n = 1 and n = 2 are found to be unstable. At lower beta (0.8%), the ballooning mode is stable; however, the 'infernal modes' are seen to persist, as shown in Fig. 15. To demonstrate the relevance of these modes, we note that when q is modified slightly, the resonances can destabilize several integer values of n. Figure 16 shows the growth rates for the case of Fig. 15, with the toroidal field scaled so that the q-axis changes from 1.05 to 0.96. We note that in this situation several integer n-values are simultaneously destabilized.

The 'infernal modes' add a new wrinkle to the estimation of beta limits. Traditionally, beta limits have been calculated from an analysis of the n = 1 external kink instability and the high-n ballooning instability; low-n and intermediate-n modes have been largely ignored. This study indicates that such an approach may not be adequate. To illustrate this, we determine the beta limit for a toroidal mode number near the peak of the resonance, between n = 1 and n = 2, i.e. n ~ 1.8, for the sequence of q-profiles studied in Figs 5–10. This beta limit is compared with that of the high-n ballooning mode in Fig. 17. For $\alpha_q > 2$, the low-n mode is seen to have a significantly lower threshold. We also note that in this case the toroidal mode numbers with n corresponding to the higher resonances have thresholds which lie between that for n = 1.8 and n = ∞. The region between the two curves marks the domain of the 'infernal mode'. Finally, Figs 18 and 19 show plots of the displacement vector field for two typical 'infernal modes', with n = 3 and n = 7. The low-n mode is seen to be broad

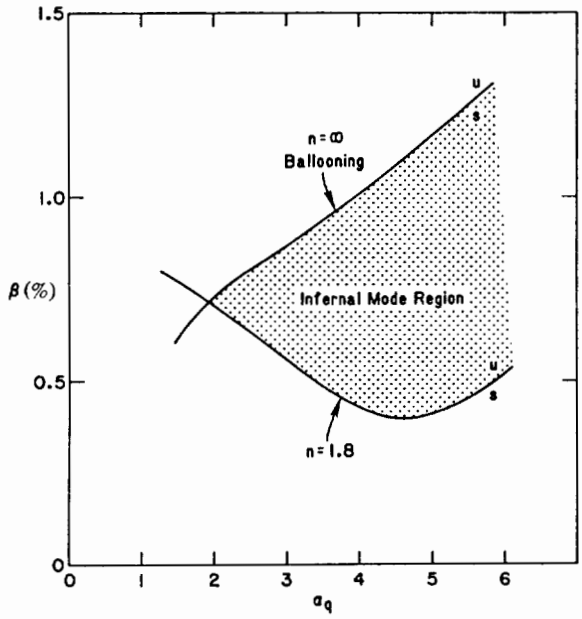

FIG. 17. Variation of the beta limit with the shear parameter α_q for the infinite-n ballooning mode and for the mode with n = 1.8. The region of instability for each mode lies above the corresponding curve. The hatched region identifies the domain of the 'infernal mode'.

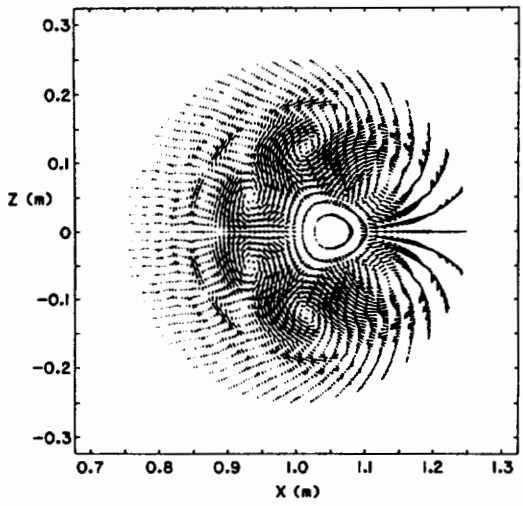

FIG. 18. Projection of the unstable displacement vector onto the x–z plane, for the case with α_q = 3.0, β = 1.5%, and toroidal mode number n = 3.0.

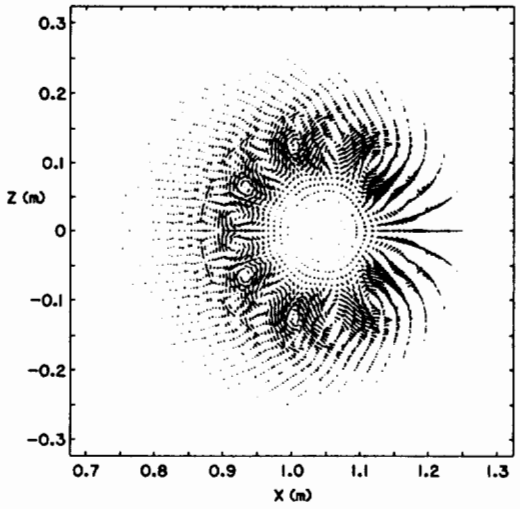

FIG. 19. Displacement vector for the same equilibrium as in Fig. 18, with toroidal mode number n = 7.0.

in its radial extent and may be expected to affect the plasma drastically. The higher-n mode is, however, more localized in its radial extent and the usual understanding of the ballooning mode may apply here.

4. DISCUSSION

Pressure driven internal modes in tokamaks have been shown to exhibit a rich complexity if the global shear is weak. Hastie and Taylor [19] have pointed to this in their work and identify two regimes of interest. When n and q′ satisfy the relation $n \gg (\psi q')^{-2} \gg 1$, Hastie and Taylor predict that the standard ballooning theory is valid. When the shear is reduced, so that $(\psi q')^{-2} \gg n \gg 1$, they find that there is a need for their new theory. The significant features of their theory are that the growth rate will be an oscillatory function of n with decreasing amplitude and that, when n is large enough to recover the first condition, the results match the standard ballooning theory. The period of the oscillations is predicted to be constant in n ($\Delta n \sim 1/q$), but the amplitude decreases as $1/n^2$. To determine the region of validity of each of these theories, we plot in Fig. 20 $(\psi q')^{-2}$ as a function of the radial location in the plasma for different values of α_q. Since the gradient in the pressure profile peaks at $\psi \sim 0.2$, it is relevant to concentrate on that surface. We note that for $\alpha_q \leq 2$ at $\psi = 0.2$ the value of $(\psi q')^{-2}$ is about 1, and we might expect the standard theory to be valid for all $n \gg 1$. This is supported by the results of Figs 3–6. As α_q is increased from 2 to 3, $(\psi q')^{-2}$ increases sharply from 1.5 to 15. This gives us the conditions to test the Hastie–Taylor theory. In fact, when $\alpha_q = 2.5$, we have observed that when n is greater than 10, the oscillations in $\omega^2(n)$ are damped and a monotonic variation is recovered, as predicted. This is partly shown in Fig. 7, which is restricted to $n < 8$, but clearly shows a diminishing oscillation amplitude. The reduction in the amplitude does not exactly match the predictions of the Hastie–Taylor theory. At small values of n, the amplitude decreases slower than 1/n, and, as n is increased, it approaches the predicted $1/n^2$. However, for $\alpha_q > 3$, we see no evidence of a reduction in the amplitude of the oscillation and even the Hastie–Taylor theory breaks down as we enter the 'infernal mode' regime. It is important to note that it is the value of $(\psi q')^{-2}$ at the surface of largest p′ that matters, not α_q itself. This is evident from the results of Fig. 11, where p′ was chosen to peak at $\psi = 0.9$, a surface at which $(\psi q')^{-2} \ll 1$. For this case we note an absence of the oscillations in $\omega^2(n)$.

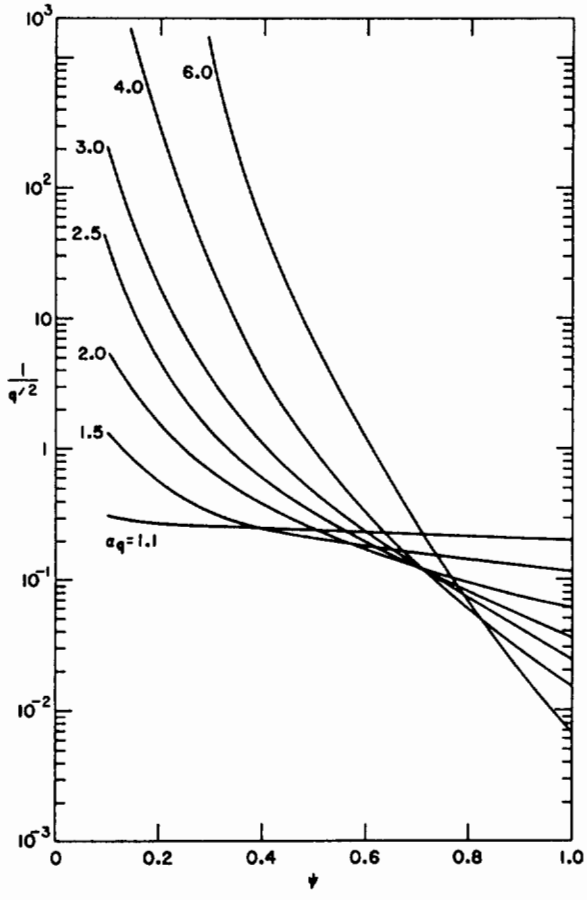

FIG. 20. Plots of $(q')^{-2}$ versus ψ for different α_q. Standard ballooning theory is valid for n well above the appropriate curve.

charges for a possible connection with 'infernal mode' activity. Unfortunately, the experimental data rarely provide detailed information on the q-profile — a fundamental requirement for this sort of analysis. Finally, we note that these instabilities may play a major role in ignited plasmas, where all the required plasma conditions may be present. To avoid them, it will be necessary to maintain finite shear in the interior of the plasma or to broaden the pressure profile so that the pressure gradients are minimal in regions of low shear.

ACKNOWLEDGEMENTS

The authors wish to acknowledge the invaluable assistance of Mr. A.E. Miller in running the PEST code for this study.

This work was supported by the United States Department of Energy, under Contracts Nos. DE-AC02-76-CHO-3073 and DE-FG02-86ER-53226.

REFERENCES

[1] WESSON, J.A., Nucl. Fusion **18** (1978) 87.
[2] FREIDBERG, J.P., Rev. Mod. Phys. **54** (1982) 801.
[3] TODD, A.M.M., MANICKAM, J., OKABAYASHI, M., CHANCE, M.S., GRIMM, R.C., GREENE, J.M., JOHNSON, J.L., Nucl. Fusion **19** (1979) 743.
[4] BERNARD, L.C., MOORE, R.W., Phys. Rev. Lett. **46** (1981) 1286.
[5] YAMAZAKI, K., AMANO, T., NAITOU, H., HAMAD, Y., AZUMI, M., Nucl. Fusion **25** (1985) 1543.
[6] KERNER, W., GAUTIER, P., LACKNER, K., SCHNEIDER, W., GRUBER, R., TROYON, F., Nucl. Fusion **21** (1981) 1383.
[7] GREENE, J.M., CHANCE, M.S., Nucl. Fusion **21** (1981) 453.
[8] MANICKAM, J., Nucl. Fusion **24** (1984) 595.
[9] CHANCE, M.S., JARDIN, S.C., STIX, T.H., Phys. Rev. Lett. **51** (1983) 1963.
[10] MANICKAM, J., GRIMM, R.C., OKABAYASHI, M., Phys. Rev. Lett. **51** (1983) 1959.
[11] DOBROTT, D., NELSON, D.B., GREENE, J.M., GLASSER, A.H., CHANCE, M.S., FRIEDMAN, E.A., Phys. Rev. Lett. **39** (1977) 43.
[12] CONNOR, J.W., HASTIE, R.J., TAYLOR, J.B., Phys. Rev. Lett. **40** (1978) 396.
[13] COPPI, B., FERREIRA, A., RAMOS, J.J., Phys. Rev. Lett. **44** (1980) 990.
[14] GRIMM, R.C., GREENE, J.M., JOHNSON, J.L., Methods Comput. Phys. **16** (1976) 253.
[15] GRUBER, R., TROYON, F., BERGER, D., et al., Comput. Phys. Commun. **21** (1981) 323.
[16] DEWAR, R.L., MANICKAM, J., GRIMM, R.C., CHANCE, M.S., Nucl. Fusion **21** (1981) 493.
[17] CHARLTON, L.A., DORY, R.A., PENG, Y.-K.M., et al., Phys. Rev. Lett. **43** (1979) 1395.
[18] TAYLOR, J.B., Phys. Bl. **35** (1979) 611.
[19] HASTIE, R.J., TAYLOR, J.B., Nucl. Fusion **21** (1981) 187.
[20] DeLUCIA, J., JARDIN, S.C., TODD, A.M.M., J. Comput. Phys. **37** (1980) 183.
[21] GRIMM, R., DEWAR, R.L., MANICKAM, J., J. Comput. Phys. **49** (1983).
[22] STRAUSS, H.R., PARK, W., MONTICELLO, D.A., WHITE, R.B., JARDIN, S.C., CHANCE, M.S., TODD, A.M.M., GLASSER, A.H., Nucl. Fusion **20** (1980) 638.

(Manuscript received 21 April 1987
Final manuscript received 8 July 1987)